Genetic Algorithm-Based RF Synchronization Under Harsh Wireless Conditions for Multi-Class UAV Systems

Farhan Ali, *Senior Member, IEEE*, Rui Zhang, *Member, IEEE*, and Zhi Quan, *Senior Member, IEEE*

***Abstract*—This letter presents a robust genetic algorithm (GA)-based synchronization framework that integrates RF time-of-arrival observations with GA-based clock-offset and drift estimation. The GA operates directly in the nonlinear timing domain and remains robust to corrupted, sparse, and highly variable RF measurements. A lightweight forward-backward Kalman smoother subsequently attenuates residual noise. Extensive simulations under clean, heavy-rain, heavy-snow, high-wind, and thunderstorm conditions demonstrate that the GA substantially reduces synchronization errors across all environments. These results show that the proposed framework provides dependable, computationally efficient clock synchronization for autonomous multi-class UAV systems operating under harsh wireless conditions.**

***Index Terms*—Clock drift and offset, genetic algorithm, genetic search, harsh wireless environments, RF synchronization.**

I. Introduction

UAV communications have recently emerged as a key technology for flexible network deployment [1], [2] and are particularly important in low-altitude airspace. Accurate and reliable synchronization is a key challenge in UAV networks, as each UAV operates on its own local clock that can gradually drift and become offset over time. This challenge worsens in practical scenarios where RF communication is degraded by noise, multipath fading, and packet loss, making accurate time synchronization difficult. Conventional synchronization methods assume stable communication links and Gaussian noise models. However, these assumptions do not always hold in UAV environments, where conditions can be dynamic, unpredictable, harsh, and non-ideal. Genetic algorithms (GAs) have demonstrated considerable success in applied domains, particularly in complex, high-dimensional spaces, across various UAV applications, including trajectory design, path planning, and resource allocation. Accordingly, we adopt a GA because its global search capability and robustness to nonconvexity and missing data make it well suited to estimating clock offset and drift from imperfect RF measurements. However, conventional GA methods often suffer from slow convergence and premature stagnation. Several improvements have been proposed to overcome this issue, including Bayesian-guided GA [3], meta-learning GA (MLGA) [4], BAS-GA hybrids [5], simulated-annealing-assisted GA [6], MLGA-based routing [7], chaos-based initialization [8], and route optimization strategies [9]. Additional works include guided GA for routing [10], cluster-based methods [11], GA-neighborhood search hybrids [12], and hybrid GA-simulated annealing techniques [13], demonstrating the effectiveness of GA-based optimization in complex UAV scenarios. Recent synchronization research has also explored sensing-assisted [14] and ELM-based techniques [15] for dynamic wireless environments.

Despite these advancements in UAVs, existing solutions focus on navigation and task optimization, largely ignoring wireless timing impairments that directly affect coordinated UAV operations. The methods in [3]– [13] generally assume reliable communication links or ignore timing distortions caused by RF fading, jitter, packet loss, and non-Gaussian noise. To address these limitations, we propose a GA-based RF synchronization framework with forward-backward (FB) Kalman smoothing for joint clock offset and drift estimation that outperforms least squares (LS), the Kalman filter, and recursive least squares (RLS) under diverse RF impairments. To the best of our knowledge, prior work has not simultaneously applied per-node GA optimization to RF measurements and FB Kalman smoothing for online synchronization. The framework is a practical and reliable solution for operating UAVs in adverse RF environments. The main contributions of this work are as follows:

- A robust synchronization framework is developed for large-scale UAV networks, where RF time-of-arrival measurements are used to estimate and correct clock offset and drift in real time. The framework is designed to operate at one-second update intervals over long mission durations without relying on a Global Navigation Satellite System (GNSS) or offline processing. To ensure realistic evaluation, the framework incorporates a channel model that captures clear weather, strong winds, heavy rain, snow, and thunderstorms, which introduce varying levels of noise, packet loss, fading, and interference similar to those in real-world UAV scenarios.
- A robust GA estimation approach is proposed, combining a compact GA-based estimator with a lightweight FB Kalman smoothing stage. The GA estimator reliably estimates clock offset and drift from noisy, sparse, and intermittent measurements and includes a stable

This work was supported by the National Natural Science Foundation of China under Grant 62471311. *(Corresponding author: Rui Zhang.)*

The authors are with the State Key Laboratory of Radio Frequency Heterogeneous Integration, Guangdong Provincial Key Laboratory of Intelligent Information Processing, and College of Electronics and Information Engineering, Shenzhen University, Shenzhen 518060, China (e-mail: farhanali@szu.edu.cn; zhrrygh@szu.edu.cn; zquan@szu.edu.cn).

fallback mechanism in low-data scenarios. Furthermore, the smoothing stage refines clock synchronization by reducing residual jitter and suppressing outliers, enabling consistent performance at a modest computational cost suitable for real-time deployment.

II. Theoretical Framework

A. Clock and RF Measurement Model

Recent studies have shown that UAV air-to-ground (A2G) channels are inherently nonstationary because of changes in propagation geometry, mobility, and platform stability, which lead to time-varying delays, fading, and channel characteristics [16], [17]. Furthermore, measurement-based studies have reported significant variations in delay spread, fading, and shadowing along UAV flight paths [18]. Motivated by these channels, the channel model in this paper accounts for nonstationary channel dynamics that cause time-varying delays, fading, packet loss, and interference, which are further intensified under harsh weather conditions. The proposed work incorporates these effects through dynamic RF impairments, including delay jitter, fading variations, noise fluctuations, and burst interference, thereby providing a realistic environment for evaluating UAV clock synchronization algorithms. The intrinsic clock of UAV i is modeled as

$$c_i(t_k) = t_k + \theta_i + \gamma_i t_k + \eta_i(t_k), \tag{1}$$

where θ_i denotes the clock offset, γ_i represents the normalized fractional frequency drift, and $\eta_i(t_k)$ captures small residual variations over time. The RF master transmits timestamp t_k, which UAV i receives after the propagation delay

$$\tau_i = \bar{\tau} + \delta_i. \tag{2}$$

Around this nominal delay, harsh RF and weather conditions introduce short-term distortions:

$$\Delta_i(t_k) = \xi_i(t_k) + \phi_i(t_k) + \nu_i(t_k). \tag{3}$$

The observed RF timing error is affected by fading-induced bias, occasional impulsive interference, jitter, and receiver noise $n_i(t_k)$, giving

$$z_i(t_k) = c_i(t_k) - (t_k + \tau_i + \Delta_i(t_k)) + n_i(t_k). \tag{4}$$

Substituting (1)–(3), all channel-induced distortions combine into a disturbance $w_i(t_k)$, giving the compact linear model. The nominal propagation delay τ_i is absorbed into the effective offset estimate and is not explicitly compensated; therefore, residual inter-UAV biases associated with link-dependent propagation delays may remain.

$$z_i(t_k) = \theta_i + \gamma_i t_k + w_i(t_k). \tag{5}$$

The term $w_i(t_k)$ denotes the aggregate disturbance affecting the RF-based measurements. It accounts for multiple sources of error, including receiver noise, RF fading, occasional interference, and propagation-delay variations. Because of impulsive disturbances, the resulting noise is non-Gaussian and heavy-tailed, with large deviations occurring more frequently. Furthermore, packet drops make measurements unavailable at some time instants. As a result, only the subset of valid observations denoted by Ω_i is used for estimation. This reflects the practical constraints of operating under incomplete and unreliable measurement conditions.

B. Genetic-Drift Estimator

Traditional least-squares and Kalman-based methods remain effective under structured observations but may require additional tuning or adaptation under sparse and heterogeneous RF conditions. To address this, we use a **GA** to estimate offset and drift.

For UAV i, define the cost

$$J_i(\theta,\gamma) = \frac{1}{|\Omega_i|} \sum_{k\in\Omega_i} \left(z_i(t_k) - \theta - \gamma t_k\right)^2. \tag{6}$$

The proposed GA optimizes clock offset and drift, requiring approximately 3,200 fitness evaluations per UAV (approximately 80,000 for 25 UAVs), making it suitable for embedded UAV platforms. The GA maintains a population of candidate pairs (θ,γ) within bounded ranges and evolves them using (1) elite selection, (2) crossover, (3) Gaussian mutation, and (4) range clamping. The GA solution is

$$(\hat{\theta}_i, \hat{\gamma}_i) = \arg\min_{\theta,\gamma} J_i(\theta,\gamma). \tag{7}$$

The model follows the standard clock representation, in which the measurement is expressed as the sum of offset, drift, and a combined disturbance term that accounts for noise and channel effects. The corrected clock is obtained by estimating the offset and drift, yielding a simple and practical solution. The GA is naturally robust to fading, missing data, and impulsive interference, making it a reliable estimator that can maintain synchronization and stable clock correction even under challenging RF conditions.

$$\tilde{c}_i(t_k) = c_i(t_k) - \hat{\theta}_i - \hat{\gamma}_i t_k. \tag{8}$$

Initially, the RF measurements are corrupted by non-Gaussian disturbances such as fading, interference, and packet loss, which are handled by the GA estimation stage. After the dominant offset and drift are removed, the residual error becomes sufficiently small to be reasonably approximated by a Gaussian distribution, making it suitable for efficient refinement using a Kalman smoothing model. Residual noise is removed using a lightweight scalar state model:

$$x_i(t_{k+1}) = x_i(t_k) + w_k, \qquad w_k \sim \mathcal{N}(0, q\Delta t), \tag{9}$$

$$\tilde{c}_i(t_k) = x_i(t_k) + v_k, \qquad v_k \sim \mathcal{N}(0, r_i), \tag{10}$$

with r_i estimated from the residual variance. In (9) and (10), the process noise w_k and measurement noise v_k are modeled as zero-mean Gaussian random variables with covariances $q\Delta t$ and r_i, respectively. It is important to note that w_k and v_k represent only the **residual noise after GA correction**; they do **not** account for the earlier heavy-tailed disturbances, which have already been removed. A forward filter provides online estimation of the GA-corrected clock, while a backward smoother refines these estimates using future measurements, reducing residual jitter and suppressing outliers. This two-stage approach ensures robust and accurate synchronization under noisy, intermittent RF conditions. The degradation under thunderstorm conditions is due to stronger interference and temporal variability that limit the accuracy of the random-walk smoothing model in (9) and (10), leading to suboptimal refinement after GA correction, while the GA stage still performs well in other conditions.

$$\hat{x}_i(t_k) = \text{FB-Smooth}\{\tilde{c}_i(t_k)\}, \tag{11}$$

producing the final synchronized timeline.

C. Simulation Environment

The simulation models a 20-minute UAV mission sampled at 1 Hz (1201 steps) with 25 UAVs, each initialized with a clock offset drawn from $\mathcal{N}(0, 0.5^2)$ s and a base drift drawn from $\mathcal{N}(0, 0.01^2)$ s/s. To evaluate the proposed synchronization algorithm under varying channel conditions, we adopt a channel model that modulates the base clock-drift standard deviation using environment-specific scaling factors. The factors (Clean = 1.0, Heavy Snow = 1.5, Heavy Rain = 1.3, Heavy Wind = 1.1, and Thunderstorm = 2.0) reflect increasing levels of environmental impairment. These values are chosen to capture relative effects on algorithm performance and to provide a consistent means of benchmarking performance under adverse conditions, based directly on the simulation framework implemented in our work. RF propagation includes a per-UAV delay with a mean of 0.030 s and a standard deviation of 0.005 s, plus jitter of 0.001 s. Each environmental class imposes its own RF impairment parameters: receiver-noise variance, packet-drop probability, fading-delay variance, glitch probability, and impulsive-interference strength. The environmental RF impairment parameters were physically motivated by representative UAV A2G channel studies [18], [19] and weather-related propagation recommendations [20]. GA synchronization uses a 40-member population, 80 generations, 8 elites, a mutation probability of 0.2, and bounded search ranges of ± 40 s (offset) and ± 0.05 s/s (drift), requiring at least 30% valid RF samples. A lightweight 1-D FB Kalman smoother is applied with process noise 10^{-4}, a measurement-noise floor of 10^{-6}, and residual-based variance estimation. Performance is evaluated using per-UAV RMSE/MAE, time-resolved fleet RMSE, and per-class median recovery. The GA optimizes only offset and drift. With $P = 40$, $G = 80$, and $M \leq 1200$, the computational cost is approximately 3.8×10^6 operations per UAV (approximately 9.6×10^7 for 25 UAVs), which is negligible. Runtime on an Intel Core i5 is approximately 0.32 s per UAV (approximately 8 s total), corresponding to less than 0.7% of a 20-minute mission and confirming real-time feasibility. Algorithm 1 and Fig. 1 summarize the complete execution flow of the proposed RF-Genetic synchronization framework.

III. Results and Discussion

Table I reports per-class synchronization recovery relative to the baseline under different RF and weather conditions. RF-Genetic maintains the highest recovery across all classes (97–100%), while LS is also strong in Clean, Heavy Snow, Heavy Rain, and Heavy Wind (96–99%) but drops to 85% under Thunderstorm. RLS and Kalman remain stable, whereas RF-Genetic+FB shows a severe drop to 70% under Thunderstorm.

Fig. 2 reports the per-class median RMSE of each method under harsh weather conditions. The results show that all syn-

Algorithm 1 Proposed RF-Genetic+FB Synchronization Framework

Require: Reference timestamps, number of UAVs N_d, RF impairment parameters, GA parameters $(P = 40, G = 80)$
Ensure: Synchronized UAV clocks
  Generate UAV clock trajectories with random offset θ_i and drift γ_i
  Apply RF channel effects: propagation delay, jitter, fading, packet loss, and interference
  Construct observed RF timing error $z_i(t_k)$
  for $i = 1$ to N_d **do**
    Initialize GA population for UAV i
    Evaluate fitness based on synchronization error
    Perform selection, crossover, and mutation
    Estimate offset $\hat{\theta}_i$ and drift $\hat{\gamma}_i$
    Correct UAV clock using $\hat{\theta}_i$ and $\hat{\gamma}_i$
    Estimate residual variance r_i
    Apply forward Kalman filtering
    Apply backward smoothing
    Obtain refined synchronized clock
  end for

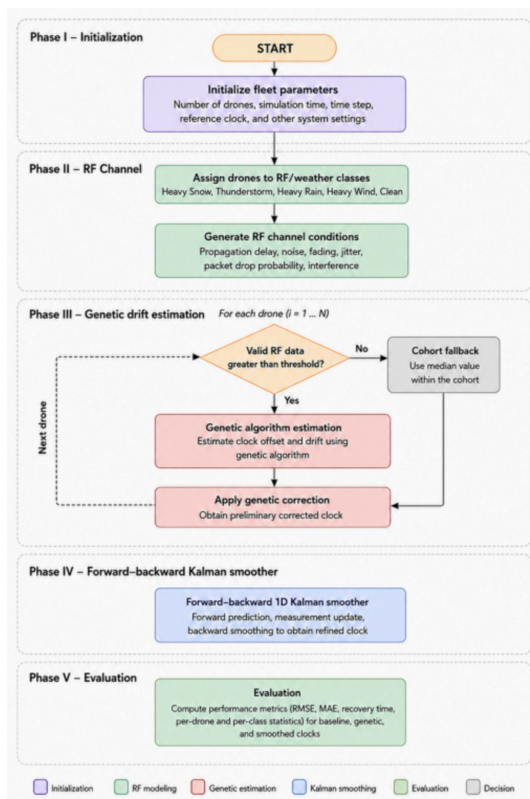

Fig. 1. Flowchart of the proposed algorithm.

TABLE I
EACH-CLASS SYNCHRONIZATION RECOVERY RELATIVE TO THE BASELINE UNDER DIFFERENT RF CHANNEL CONDITIONS.

Class	LS	RLS	Kalman	RF-Genetic	RF-Genetic+FB
Clean	99%	93%	99%	100%	99%
Heavy Snow	97%	94%	91%	99%	95%
Heavy Rain	96%	93%	93%	99%	95%
Heavy Wind	96%	94%	91%	98%	97%
Thunderstorm	85%	90%	89%	97%	70%

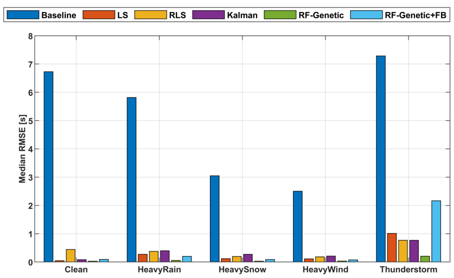

Fig. 2. Per-class median RMSE by method under harsh weather conditions.

chronization methods substantially reduce the baseline error, with RF-Genetic achieving the lowest RMSE across most weather conditions, while RF-Genetic+FB degrades under Thunderstorm because of severe RF packet corruption.

Fig. 3 provides the RMSE distribution of each method across all UAVs. The baseline errors grow significantly, reflecting heterogeneous drift and RF conditions. RF-Genetic uniformly suppresses these errors and stabilizes the estimates, yielding RMSE values close to zero and lower than those of RF-Genetic+FB, LS, RLS, and the Kalman filter.

Fig. 4 shows the time-resolved RMSE, comparing the baseline with all methods and illustrating the evolution of fleet-wide RMSE over the full mission. The baseline error grows linearly with time because clock drift accumulates without correction. In contrast, RF-Genetic immediately suppresses the error to near-zero levels and maintains stability throughout the mission. The Kalman filter, LS, and RLS perform reasonably under all conditions but degrade sharply in harsh environments. The RF-Genetic+FB smoother introduces a short transient as the filter converges and a small rise near the end because of estimated measurement-noise-floor effects, but it remains well below the baseline overall. To avoid boundary effects associated with the reduced availability of future observations near the end of the window, RF-Genetic+FB results are reported only up to $t = 1170$ s.

Table II summarizes fleet-level median synchronization accuracy across all UAVs. The baseline has the largest error (RMSE/MAE = 6.0494/5.2493 s), while LS, RLS, Kalman, RF-Genetic, and RF-Genetic+FB reduce it to 0.1360/0.0949 s, 0.4385/0.4218 s, 0.2742/0.2146 s, 0.0413/0.0352 s, and 0.1250/0.0436 s, achieving improvements of 97.8%, 92.8%, 95.5%, 99.3%, and 97.9%, respectively.

Table III summarizes the per-class median RMSE across UAV conditions. The proposed RF-Genetic method achieves the lowest RMSE in all conditions, i.e., Clean (0.0314 s),

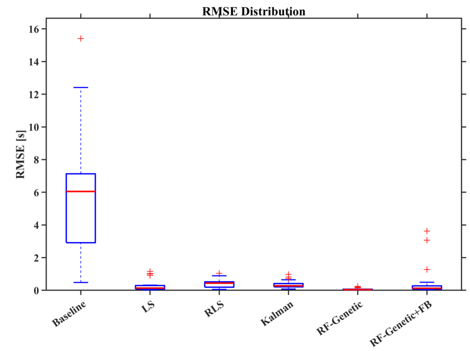

Fig. 3. RMSE distribution of each method.

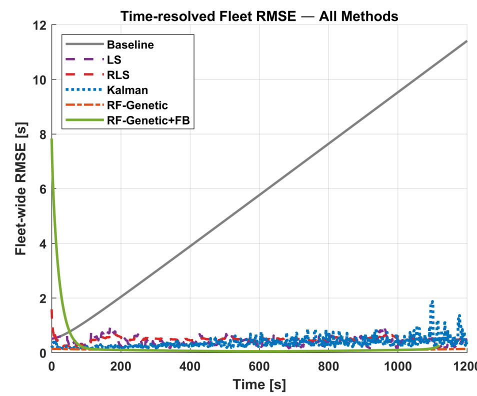

Fig. 4. Time-resolved RMSE: comparison of baseline with all methods.

TABLE II
FLEET-WIDE MEDIAN SYNCHRONIZATION PERFORMANCE ACROSS ALL UAVS.

Method	RMSE (s)	MAE (s)	Improvement
Baseline	6.0494	5.2493	–
LS	0.1360	0.0949	+97.8%
RLS	0.4385	0.4218	+92.8%
Kalman	0.2742	0.2146	+95.5%
RF-Genetic	0.0413	0.0352	+99.3%
RF-Genetic+FB	0.1250	0.0436	+97.9%

TABLE III
PER-CLASS MEDIAN RMSE ACROSS UAV WEATHER CONDITIONS.

Condition	Baseline	LS	RLS	Kalman	RF-Genetic	RF-Genetic +FB
Clean	6.7284	0.0454	0.4456	0.0818	0.0314	0.0910
Heavy Snow	3.0505	0.1202	0.1945	0.2742	0.0275	0.0883
Heavy Rain	5.8142	0.2729	0.3746	0.3981	0.0556	0.2025
Heavy Wind	2.5045	0.1106	0.1810	0.2108	0.0335	0.0725
Thunderstorm	7.2846	1.0138	0.7690	0.7690	0.2038	2.1672

Heavy Snow (0.0275 s), Heavy Rain (0.0556 s), Heavy Wind (0.0335 s), and Thunderstorm (0.2038 s). LS, RLS, and Kalman also reduce the baseline error, but their RMSE values increase under Thunderstorm to 1.0138 s, 0.7690 s, and 0.7690 s, respectively, while RF-Genetic+FB degrades sharply to 2.1672 s. The RF-Genetic+FB variant yields slightly smaller improvements under moderate conditions (e.g., Clean and Heavy Snow), but it exhibits increased residual errors in

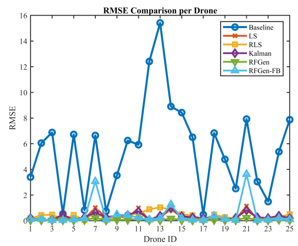

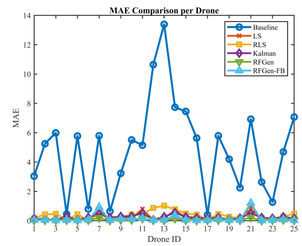

Fig. 5. RMSE comparison per UAV.

Fig. 6. MAE comparison per UAV.

severe environments such as Thunderstorm, indicating that **FB smoothing may not always yield benefits in highly adverse scenarios**. Overall, the GA achieves substantial error reduction while maintaining reliable performance under varying channel conditions.

As shown in Figs. 5 and 6, baseline timing errors across all UAVs and channel classes range from 3–16 s and 3–14 s, reflecting heterogeneous drift behavior under harsh RF conditions. The RF-Genetic estimator reduces these errors, indicating stable recovery even when RF observations are sparse or distorted. The results show per-UAV robustness and indicate that the proposed synchronization framework scales across heterogeneous UAV operating conditions. These figures show that RF-Genetic uniformly suppresses these errors and further stabilizes the estimates, yielding RMSE values close to zero for most UAVs and consistently achieving the lowest RMSE and MAE values. LS and the Kalman filter also achieve significant improvements, with lower RMSE and MAE. In the RF-Genetic+FB and RLS cases, a few UAVs with extremely sparse or corrupted RF observations exhibit slightly higher errors, consistent with the fallback and smoothing noise-variance estimation. However, RF-Genetic+FB still shows competitive performance with occasional error spikes. The GA performs better than LS, Kalman, RLS, and RF-Genetic+FB in all cases, demonstrating strong scalability and per-UAV consistency of the proposed method.

IV. Conclusion

This letter introduces a robust GA-based RF synchronization framework for UAV fleets operating in severe environments with rapidly varying channel conditions. The framework integrates a GA search-based estimator for clock offset and drift with a lightweight FB Kalman smoother to recover RF timing measurements from distorted, sparse, and non-Gaussian data without hardware assumptions. The simulation results show that the GA achieves significant improvements across multiple RF and harsh weather conditions, reducing synchronization error relative to the baseline, LS, Kalman, RLS, and RF-Genetic+FB, thereby stabilizing performance across all UAV conditions. The results of the per-class and per-UAV analyses demonstrate that the methodology is robust to jitter, fading, impulsive interference, and packet drops. This framework provides a reliable, high-precision, and effective synchronization solution for coordinated multi-class UAV systems that use only noisy RF timestamps, maintaining strong reliability even in challenging conditions.

References

[1] D. Wu, Y. Qiu, Y. Zeng, and F. Wen, "Environment-aware channel estimation via integrating channel knowledge map and dynamic sensing information," *IEEE Wireless Communications Letters*, vol. 13, no. 12, pp. 3608–3612, 2024.

[2] W. Liu, X. Zhang, H. Xing, J. Ren, Y. Shen, and S. Cui, "UAV-enabled wireless networks with movable-antenna array: Flexible beamforming and trajectory design," *IEEE Wireless Communications Letters*, vol. 14, no. 3, pp. 566–570, 2025.

[3] Z. Zheng and H. Yao, "A method for UAV tracking target in obstacle environment," in *2019 Chinese Automation Congress (CAC)*, 2019, pp. 4639–4644.

[4] S. Xu, H. Li, and H. Gao, "A path planning method for UAV target detection based on improved genetic algorithm," in *2025 11th International Conference on Computing and Artificial Intelligence (ICCAI)*, 2025, pp. 482–486.

[5] Z. Wang, B. Wang, Y. Wei, P. Liu, and L. Zhang, "Cooperative multi-task assignment of multiple UAVs with improved genetic algorithm based on beetle antennae search," in *2020 39th Chinese Control Conference (CCC)*, 2020, pp. 1605–1610.

[6] Y. Sun and L. Fang, "Method for passive location of UAV conical formation based on genetic algorithm," in *2023 3rd International Conference on Electronic Information Engineering and Computer (EIECT)*, 2023, pp. 29–34.

[7] J. Su, J. Qi, C. Wu, M. Wang, and J. Guo, "Multi-UAVs target attack based on improved genetic algorithm," in *2020 39th Chinese Control Conference (CCC)*, 2020, pp. 1466–1471.

[8] M. Gao, Y. Liu, and P. Wei, "Opposite and chaos searching genetic algorithm based for UAV path planning," in *2020 IEEE 6th International Conference on Computer and Communications (ICCC)*, 2020, pp. 2364–2369.

[9] B. Chen and J. Huang, "Research on shortest path planning for unmanned aerial vehicles based on genetic algorithm," in *2024 IEEE 6th International Conference on Civil Aviation Safety and Information Technology (ICCASIT)*, 2024, pp. 1239–1244.

[10] Y. Li, W. Chen, B. Fu, S. Liu, L. Hao, and Z. Wu, "A distributed cooperative dynamic target search method for multi-UAV systems in complex adversarial environments," *IEEE Internet of Things Journal*, vol. 12, no. 18, pp. 38 155–38 171, 2025.

[11] M. Asim, W. K. Mashwani, S. B. Belhaouari, and S. Hassan, "A novel genetic trajectory planning algorithm with variable population size for multi-UAV-assisted mobile edge computing system," *IEEE Access*, vol. 9, pp. 125 569–125 579, 2021.

[12] Y. Zhao, D. Zhou, H. Piao, Z. Yang, R. Hou, W. Kong, and Q. Pan, "Cooperative multiple task assignment problem with target precedence constraints using a waitable path coordination and modified genetic algorithm," *IEEE Access*, vol. 9, pp. 39 392–39 410, 2021.

[13] A. N. Jasim and L. Chaari Fourati, "Guided genetic algorithm for solving capacitated vehicle routing problem with unmanned-aerial-vehicles," *IEEE Access*, vol. 12, pp. 106 333–106 358, 2024.

[14] C. Qing, Q. Zhao, N. Yang, Y. Huang, and P. Du, "Compressed ELM-based frame synchronization," *IEEE Transactions on Vehicular Technology*, vol. 73, no. 12, pp. 19 768–19 773, 2024.

[15] J. Liu, K. Mei, X. Zhang, D. McLernon, D. Ma, J. Wei, and S. A. R. Zaidi, "Fine timing and frequency synchronization for MIMO-OFDM: An extreme learning approach," *IEEE Transactions on Cognitive Communications and Networking*, vol. 8, no. 2, pp. 720–732, 2022.

[16] H. Jiang, Z. Zhang, and G. Gui, "Three-dimensional non-stationary wideband geometry-based UAV channel model for A2G communication environments," *IEEE Access*, vol. 7, pp. 26 116–26 122, 2019.

[17] M. Banagar and H. S. Dhillon, "Fundamentals of wobbling and hardware impairments-aware air-to-ground channel model," *IEEE Transactions on Vehicular Technology*, vol. 73, no. 12, pp. 17 946–17 962, 2024.

[18] X. Cai, J. Rodríguez-Piñeiro, X. Yin, N. Wang, B. Ai, G. F. Pedersen, and A. P. Yuste, "An empirical air-to-ground channel model based on passive measurements in LTE," *IEEE Transactions on Vehicular Technology*, vol. 68, no. 2, pp. 1140–1154, 2019.

[19] Z. Cui, K. Guan, C. Briso-Rodríguez, B. Ai, Z. Zhong, and C. Oestges, "Channel modeling for UAV communications: State of the art, case studies, and future directions," 2021. [Online]. Available: https://arxiv.org/abs/2012.06707

[20] International Telecommunication Union, "Specific attenuation model for rain for use in prediction methods," ITU-R, Tech. Rep. Recommendation P.838-3, 2005.